QUASI-DYNAMIC MOORING LINE MODEL

Pau Trubat*[1], Climent Molins[1], Xavi Gironella[1]

pau.trubat.casal@upc.edu, climent.molins@upc.edu, xavi.gironella@upc.edu

1. Department of Civil and Environmental Engineering, Universitat Politècnica de Catalunya (UPC BarcelonaTech), C/Jordi Girona 1-3, 08034, Barcelona, Spain

** Corresponding author*

Keywords:

mooring; model; quasi-dynamic; dynamic; FOWT; floating

ABSTRACT

The quasi-dynamic mooring line model is a new approach to assess the mooring line tension that considers the static solution of the catenary shape, but updates the distributed vertical force along the mooring line as a function of the external forces, drag and inertial, acting on the line. In this way, an updated apparent weight is applied to the static solution of the catenary shape that improves significantly the solution obtained by the quasi-static approach, with an equivalent computational cost. Then, the model improves the tension solution of the quasi-static models by using that updated weight of the mooring, achieving results much closer to the dynamic models than the standard quasi-static ones. To appraise the improvement of the results, a parametric analysis within a wide range of mooring physical parameters is conducted. The error of the quasi-static tension of one cycle is less than 20% only for the 18% of the simulations, while the quasi-dynamic model produces an error less than 20 % for the 84% of simulations. In addition, the model can predict the slack phenomenon.

1 INTRODUCTION

The modelling of mooring line dynamics has reached a high reliability from the first lumped-mass models [1][2], through the finite difference method [3–6] until the finite element models [7–12]. These models are capable to consider the full dynamics of the mooring line, the bending stiffness, the sea-bed interaction as well as the internal damping effects. However, the line should be divided into several elements, with multiple degrees of freedom as the position of the nodes and the tension along the line, which leads to models with high computational cost. On the other hand, there are also the quasi-static mooring models[13], which solve the statics of the mooring line at each time step depending on the instant fairlead position got from the platform motion. Dynamics of the mooring lines also can be estimated by analytical and empirical solutions: Gobat and Grosenbaugh proposed an empirical model to assess the dynamic tension of a mooring line due the vertical motion of it upper end [14], while Aranha & Pinto proposed an algebraic approximation to assess the dynamic tension in risers and mooring lines for harmonic excitation in the direction of the cable's tangent [15].

The Floating Offshore Wind Turbines (FOWTs) engineering models, e.g. FAST [16] and FloawDyn [17], are models for design purpose that must be fast and reliable. However, they have to consider a large number of factors that take part in the design of a FOWT like the Wind Turbine (WT), the tower vibrations, the platform hydrostatics, the mooring behavior and the definition of the met-ocean conditions. In addition, a large amount of simulations have to be performed in order to fulfil all the requirements for the Ultimate Limit State, Accidental Limit State and Fatigue Limit State of the current standards [18].

As pointed by Azcona et al. [19] and Robertson et al. [20] the mooring dynamics have little impact on the platform dynamics and its final design for a spar or a semisub platform. However, for the mooring analysis, the mooring dynamics are a key factor to determine the actual tensions on the fairleads and its variation along its service life [21,22]. Moreover, the mooring dynamics are governed mainly due to the platform motion, while other load sources like the wave forces over the moorings have little importance [23]. For design purpose, main standards such as DNV-GL [24] require a larger safety factor on the mooring line design if quasi-static analyses are performed instead of dynamic ones. Moreover, the mooring fatigue analysis has become a tough challenge due to the difficulties to assess the dynamics of mooring lines with a low computational cost that balances out the large number of simulations that have to be performed [25].

This paper presents a novel methodology, named quasi-dynamic mooring model, which assess the mooring line tension at the fairleads and anchors with high accuracy with a computational cost equivalent to the quasi-static model. The model is proposed after a thorough study of the mooring dynamics and the effects that modify the line tension while in motion. The study highlighted that the overall motion of a mooring line is mainly in vertical direction, either the motion of the fairlead is vertical or horizontal. Then, this motion produces also vertical inertia and hydrodynamic forces. These forces increase or decrease the distributed vertical resultant force (weight, inertia and hydro forces) of the line that leads to a variation of the tension at the fairlead different from the assumed by the static approach. Moreover, when the resultant forces tend to zero, the line gets slack. In this regard, Suhara et al. [26] presented a method to predict slack process from the resultant of the external forces assessed at the mid-point of the suspended segment of the mooring line. The quasi-dynamic model is based on the same principium, but accounts for the variation of the vertical distributed forces along all the suspended segment to update the static tension.

The quasi-dynamic mooring model assumes that the shape of the line in each time step is the same as the static solution for the given fairlead position. Then, the quasi-dynamic tension is assessed from the static tension by multiplying it by the quasi-dynamic factor (k_{QD}), defined as the quotient of the resultant of the vertical forces over the suspended segment mooring line (the mooring weight the inertia force and the hydrodynamic forces) between the resultant of the distributed weight. However, the model does not consider the relative motion between nodes, internal vibration, neither transverse waves in the line.

The paper is structured as follows. First, the analysis of the dynamics of a moving mooring line is presented which leads to the assumptions of the approach of the quasi-dynamic model. Second, the quasi-dynamic model approach and its implementation are presented. Third, the model is verified for a catenary line by comparing the simulations of a parametric study against a dynamic model. The parametric study consists in the analysis of the behavior of that mooring line with different line shapes, chain diameters and fairlead motion excitations. Fourth, the model is validated by comparing the simulation of the LC34 and LC43 of the DeepCwind [27] experiments studied within the OC5 project [22] and the fatigue damage is assessed and compared for each model and load case. Finally, the conclusions are presented which summarize the results obtained for the applicability of the quasi-dynamic model. Even the quasi-dynamic model presented is verified for a FOWT, the model can be applied at other offshore floating structures equipped with moorings i.e., vessels, O&G offshore rigs and wave energy converters.

2 STUDY OF THE DNAMICS OF THE MOTION OF A MOORING LINE

The dynamics of the catenary mooring line depend on the fairlead motion which is the connection point between the line and the floating body. The fairlead position defines the catenary shape as a function of the line length and the distance to the anchor. If the fairlead is motionless, the catenary line tends to its minimum energy position, the static configuration. In this configuration, the unique external forces are the weight of the mooring line, the sea-bed contact force and the anchor and fairlead reactions. The weight per meter length is the vertical downward force that gives the catenary shape to the line in absence of bending stiffness. Then, any line subjected to a constant distributed vertical force will define a catenary shape.

If a mooring line moves from an equilibrium shape with low velocity, the line tends to follow the next static catenary shapes with the corresponding tension because the other external forces, the inertial and the hydrodynamic forces are negligible. However, the larger fairlead amplitudes or frequencies, the larger external forces for cyclic motions. These forces act on the line modifying the actual tension of the fairlead, shape and motion. If the external forces are mainly horizontally, the line will lose its catenary shape quickly, but if the acting loads are mainly vertical, the catenary equations would be a good approach.

In order to get the directions of the external forces, an approximation of the motion of the shape of the mooring line is assessed for a mooring line of 13.092m length, a depth of 1.54m, a radius to anchor of 12.922, with an pretension of 6.62N, that represents a model with a scale ratio of 1:75. The Figure 1 shows the maximum amplitudes of the vertical and horizontal components for all the points of the mooring line for a horizontal motion of the fairlead(left) and for a vertical motion of the fairlead (right) of 0.03m, a motion of 0.23% of the length of the mooring line. Also, the initial shape, and the shapes for the maximum X motion, and Z motion are presented (bottom). The figure shows clearly that the main motion of all the points of the line is in vertical direction. Moreover, the amplitude of the larger vertical motion is about 10 times larger than the larger horizontal motion, even for the horizontal fairlead motion case (Figure 1 left), unless at the fairlead zone, where the horizontal motion is applied and no vertical motions is applied.

To deep on the line dynamics, the velocity and acceleration of the suspended segment of a mooring line are assessed for a cyclic horizontal motion with an amplitude of 0.0045m. The properties of the mooring line are presented at Table 1, based on the mooring lines used for the parametric study of section 4. The velocity and accelerations are assessed at four critical time points of the motion of the fairlead (Figure 2). The time points 1, 3 and 1’ are the maximum absolute velocity points, the time points 2 and 4 are the maximum absolute acceleration points. The velocity and accelerations results are assessed from a mooring line dynamics model [12] and are compared with the theoretical value get from the quasi-static model.

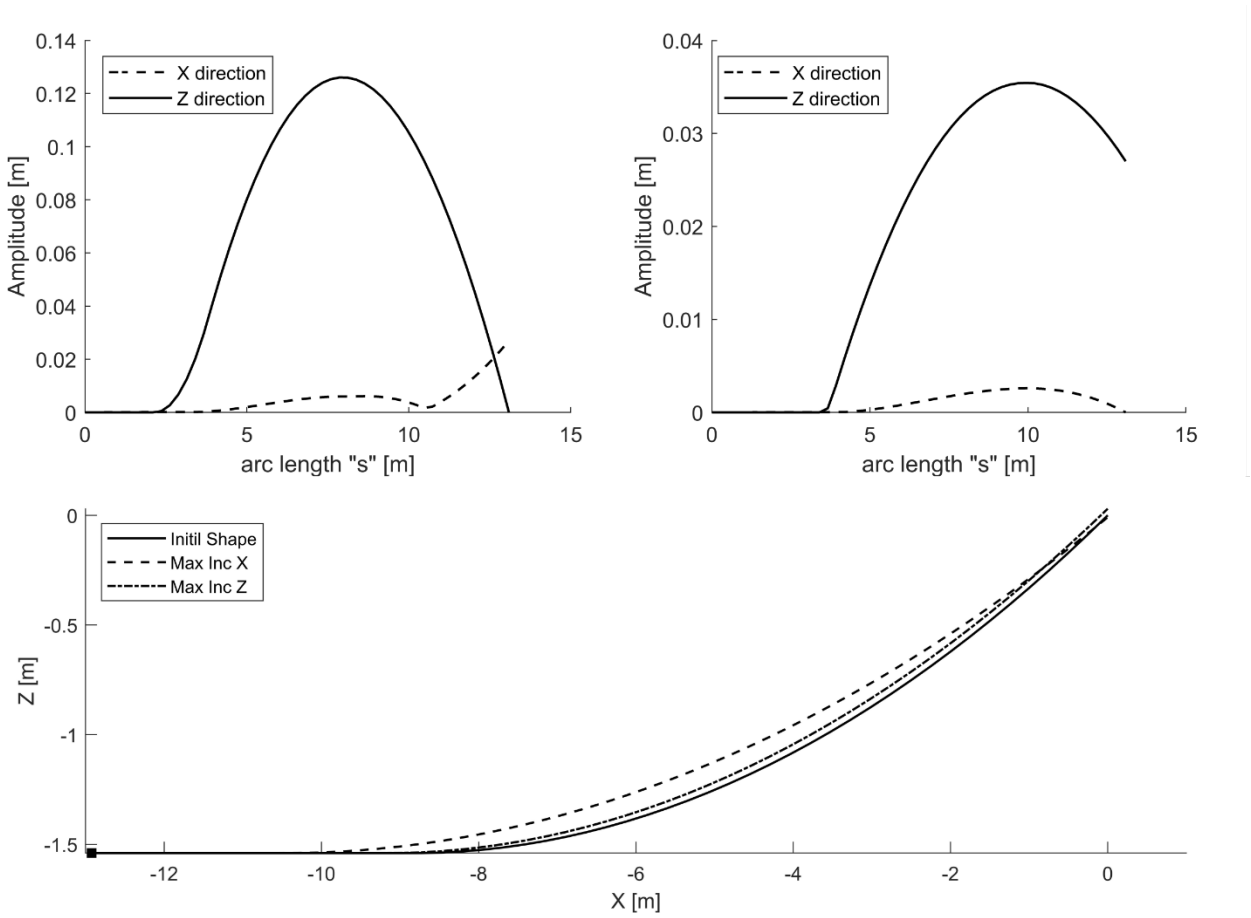

Figure 1: Quasi-static amplitude motion of a mooring line for a horizontal (left),vertical motion of the fairlead (right) and layout for initial shape and the maximum horizontal and vertical motions (bottom)

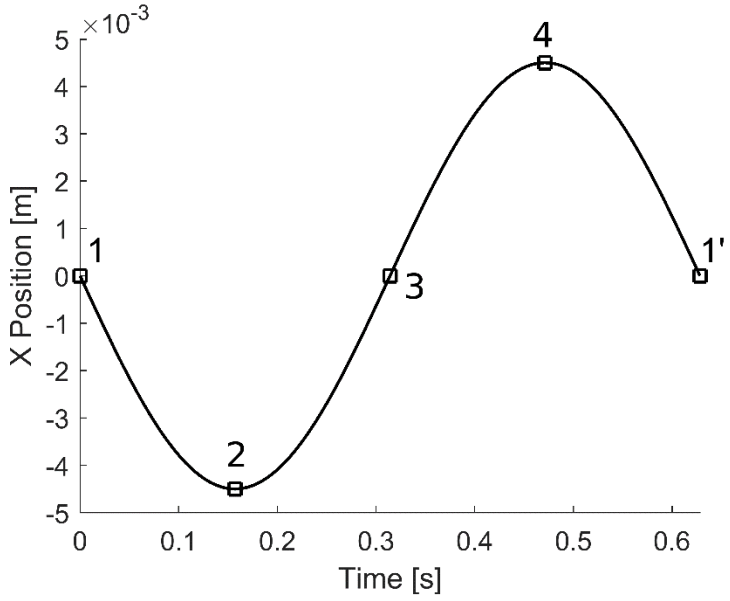

Figure 2: Fairlead position, velocity and acceleration assessment points

Table 1: Mooring line parameters based on the parametric analysis of section 4

Position of Fairlead (x,y,z) [m]	(0,0,0)
Position of Anchor (x,y,z) [m]	(-12.922,0,-1.54)
Unstretched mooring line length [m]	13.092
Diameter [mm]	1.14
Wet Weight per meter length[N/m]	0.244
EA [N]	1.17E+05

The Figure 3 shows the vector velocities and accelerations of the dynamic model along the suspended segment of the mooring line for each time point, (1, 2, 3 and 4), where the colour bar shows the magnitude of the norm of the vector. The velocity and acceleration vectors from the dynamic analysis are mainly in vertical direction, even if the motion of the fairlead is horizontal. The points closer to the fairlead present larger horizontal component, but their value is smaller than the vertical component for all the nodes. Moreover, the maximum value of the velocities and accelerations are located at the middle of the suspended segment, at the point that experiences the larger amplitude motion.

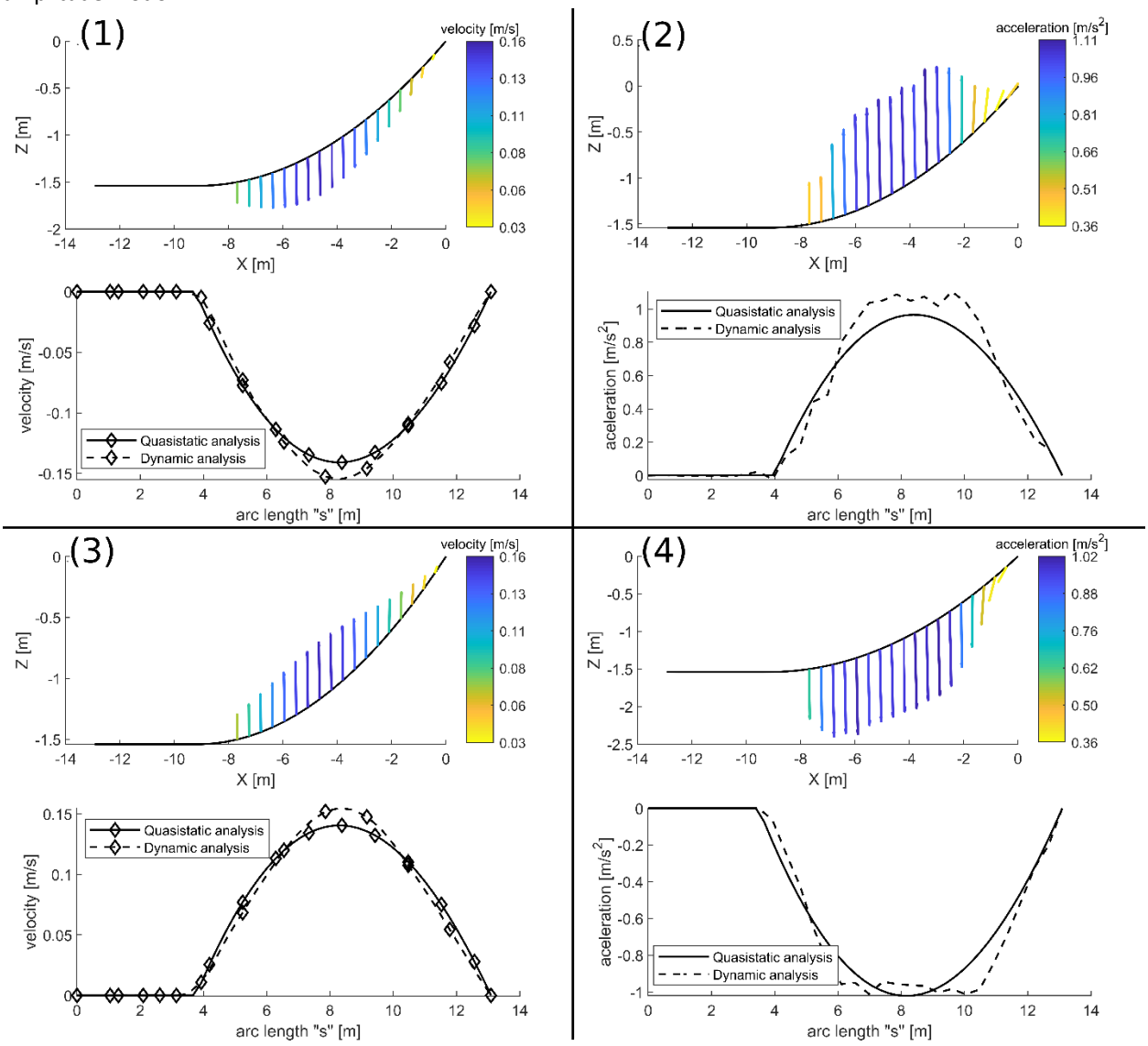

Figure 3: Quasi-static vs dynamic approach

The Figure 3 also shows the vertical component of the velocity and the acceleration depending on the time point, which are compared with the quasi-static solution. The behaviour of the quasi-static solution for the vertical component fits the dynamic one. The main differences between the simulations are found at the half of the suspended length, at the fairlead and at the touch point of the line with the seabed. These points present the maximum and minimum velocity and acceleration values. At these points are where the vertical forces differ most from the resultant mean vertical distributed load which leads to the catenary solution. Then, the catenary static solution differs slightly from the actual solution based on the dynamic analysis. Nevertheless, the mean values of the velocity and accelerations for the studied cases have little errors. The errors for the mean velocity are lower than 3.5% while the errors for the acceleration are lower than 7 %. These values support the use of the static catenary shape to approximate the velocities and accelerations of the line to assess the hydrodynamic and inertial forces. These differences will differ depending on the amplitude and frequency excitation of the fairlead. Thus, a verification analysis accounting for several amplitude and frequency magnitudes will be performed in order to assess the reliability of the proposed model. However, the quasi-static model does not account for this hydrodynamic and inertial forces to assess the tension at the fairlead.

3 MODEL APPROACH

The quasi-dynamic model approach assumes a quasi-static behavior of the mooring line by considering the catenary static shape of the line at each time step. The main difference with the quasi-static approach is that the distributed weight is updated to the apparent weight as a function of the approximation of the external forces. The apparent weight of the line is defined as the vertical distributed force of the resultant of the vertical components of the external forces (the weight, the inertial and the hydrodynamic forces).

In the proposed model, the apparent weight is applied as a quasi-dynamic factor (k_{QD}) multiplied by the static fairlead force, Eq. (1). Where the quasi-dynamic factor (k_{QD}) is assessed as the quotient of the resultant of the external forces in the vertical direction of the suspended segment between the weight of the suspended segment of the line as shown in Eq.(2). To sum up, first the static tension of the line is assessed using the distributed weight of the line, and then is updated to the quasi-dynamic tension by multiplying it for the factor k_{QD}. When the resultant vertical force is equal or larger than zero, means that the line is in slack condition and the actual tension is zero, thus the coefficient k_{QD} may be larger or equal zero. In the following equations, the variables in bold mean they are vectors in the cartesian coordinates.

$$\boldsymbol{T}_{QD} = k_{QD}\boldsymbol{T}_S \tag{1}$$

$$k_{QD} = \frac{\int_{s_0}^{l}(\boldsymbol{f}_w + \boldsymbol{f}_{HD} - \boldsymbol{f}_I)\cdot \mathbf{k}\, ds}{\int_{s_0}^{l}\boldsymbol{f}_w \cdot \mathbf{k}\, ds} \geq 0 \tag{2}$$

Where k_{QD} is the quasi-dynamic factor, $\boldsymbol{T}_{QD}$ is the quasi-dynamic tension at the fairlead, $\boldsymbol{T}_S$ is the static tension at the fairlead, $\boldsymbol{f}_w$ is the distributed weight force per unit length, $\boldsymbol{f}_{HD}$is the distributed hydrodynamic force per unit length, $\boldsymbol{f}_I$ is the inertia force, $\mathbf{k}$ is the unitary vector in z direction, s is the arc-length parameter of the mooring line, s_0 is the arc-length value of the contact point between the mooring line and the sea-bed and l is the mooring line length

3.1 Model implementation

The model requires the computation of the apparent weight. To compute it, weight, drag and inertia forces are integrated along the line by using the composite Simpson's rule integration scheme. At each point, inner velocity and acceleration of the line itself during each time step are obtained from the previous static positions of the integration points. The external forces are assessed by the second law of Newton for the inertial force and by the Morison equation, Eq. (3), for the hydrodynamic forces as shown in Figure 4. The hydrodynamic coefficients,

$C_{D,n}$and $C_{A,n}$ are the normal or transverse drag and added mass coefficients respectively, which are section dependent and can be estimated from the DNVGL-OS-301 [28]

$$\begin{aligned} \boldsymbol{f}_w &= -\omega \mathbf{k} \\ \boldsymbol{f}_I &= \rho_m A\, \mathbf{a}_i \\ \boldsymbol{f}_{HD} &= -\tfrac{1}{2}\rho_w C_{D,n} d |\mathbf{v}_i \cdot \mathbf{n}|(\mathbf{v}_i \cdot \mathbf{n})\mathbf{n} - \tfrac{\pi d_{ap}^2}{4}\rho_w C_{A,n}(\mathbf{a}_i \cdot \mathbf{n}) \end{aligned} \tag{3}$$

Where, ω is the wet weight per meter length of the line, ρ_m is the density of the mooring line material, A is the cross section of the mooring line, ρ_w is the density of the water, $C_{D,n}$ and $C_{A,n}$ are the normal drag and added mass coefficients, d is the nominal diameter of the mooring line, d_{ap} is the apparent diameter of the mooring line, $\boldsymbol{v}_i$ is the velocity of the *i-th* time step, $\boldsymbol{a}_i$ is the acceleration of the *i-th* time step, and $\mathbf{n}$ is the unitary normal vector of one point of the mooring line.

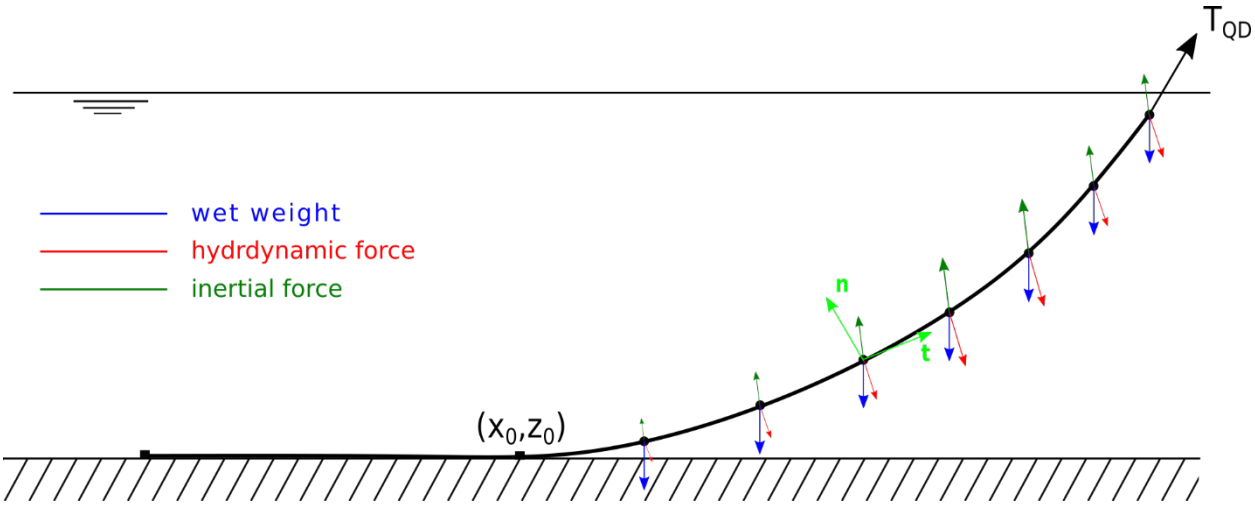

Figure 4: Mooring line discretized with dynamic forces

The procedure for assessing the quasi-dynamic forces is presented below:

1. The catenary equations [29] are assessed for the updated fairlead position for the time step *"i"*, and the positions of the nodes of the mooring lines ($\boldsymbol{r_i}$) and the static tension ($\boldsymbol{T}_s$) are obtained.
2. The velocity($\boldsymbol{v_i}$) and acceleration ($\boldsymbol{a_i}$) of the suspended nodes are assessed by Eq. (4)
3. The external forces are evaluated
4. The quasi-dynamic factor (k_{QS}) is assessed by Eq.(2)
5. The quasi-dynamic Tension is assessed by Eq. (1)
6. Compute next time step, and start again from 1

$$\begin{aligned} \mathbf{v}_i &= \frac{d\boldsymbol{r}_\mathrm{i}}{dt} \cong \frac{\Delta \mathbf{r}_i}{\Delta t} = \frac{\boldsymbol{r_i} - \boldsymbol{r_{i-1}}}{\Delta t} \\ \mathbf{a}_i &= \frac{d\mathbf{v}_i}{dt} \cong \frac{\Delta \mathbf{v}_\mathrm{i}}{\Delta t} = \frac{\boldsymbol{v_i} - \boldsymbol{v_{i-1}}}{\Delta t} \end{aligned} \tag{4}$$

4 NUMERICAL VERIFICATION

A numerical verification is performed in order to obtain the applicability of the proposed approach. The numerical verification consists of comparing the proposed model against a validated dynamic model [12]. The comparison is set for the simulations of a parametric study composed for two different chain sections and three different line shapes. The simulations consist in a forced fairlead horizontal motion for different amplitudes and frequencies that ensures a combination of horizontal and vertical motion of the line.

4.1 Parametric study

The base of the mooring configuration for the verification test is got from the configuration of the experimental set test from Suhara [26]. The variations of the mooring configurations for the parametric study are based on the scaled DeepCwind mooring system configuration [30], which has different shape and chain diameter.

The parametric study of the verification test is performed on six different mooring line configurations, composed by 2 chain diameters (D1 and D2), and 3 shapes (S1, S2 and S3). The shapes are obtained by varying the relation of the vertical span (h) versus the horizontal span from the seabed contact point (X_0) by modifying the anchor position. The mooring shape configurations have a h/X_0 relation of 0.17, 0.25, and 0.35 and are shown in Figure 5, where θ is the hang-off angle. The line characteristics with the varying parameters are presented in Table 3. The combination of the line shape and line dimaters are presented in Table 2, where the cases are named as CXY, where X is the number of the shape, and Y is the number of the chain diameter.

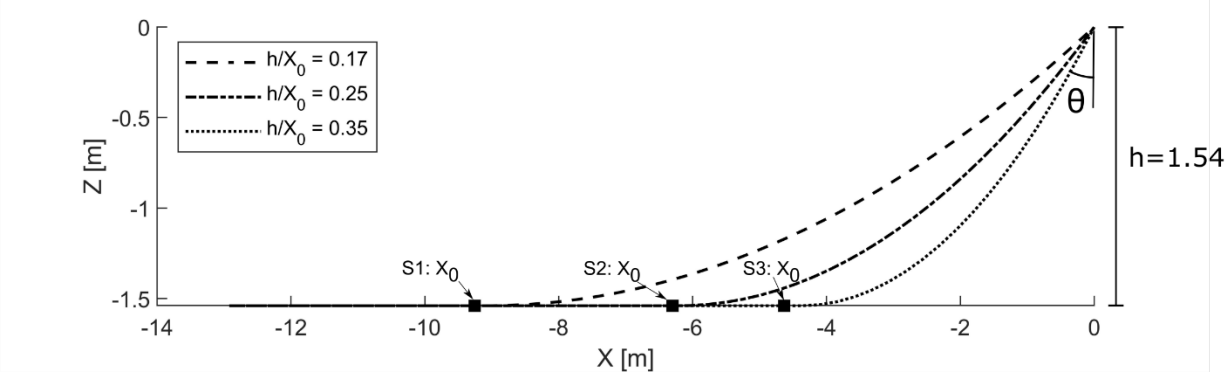

Figure 5: Catenary mooring shapes

Table 2: Parametric line shape-diameter combinations

	D1 = 1.14 mm	**D2 = 3.77mm**
S1: h/ X_0 = 0.17	C11	C12
S2: h/ X_0 = 0.25	C21	C22
S3: h/ X_0 = 0.35	C31	C32

Table 3: Mooring line characteristics

Position of Fairlead (x,y,z) [m]		(0,0,0)
Depth of the Anchor		1.54
Anchor Horizontal Position [m]	**S1**	-12.922
	S2	-12.845
	S3	-12.75
Hang Off angle (θ) [deg]	**S1**	18.9
	S2	26.8
	S3	36.1
Mooring line type		Chain
Unstretched mooring line length [m]		13.092
Diameter [mm]	**D1**	1.14
	D2	3.77
Wet Weight per meter length[N/m]	**D1**	0.244
	D2	1.98
Mass per unit length [kg/m]	**D1**	0.028
	D2	0.23
Stiffness EA [N]	**D1**	1.17E+05
	D2	1.28E+06
Normal drag coefficient Cdn		2.5
Added mass coefficient Ca		1
Seabed stiffness [N/m^2]		1E+05
Number of nodes in the dynamic model		31
Integration points for the quasi-dynamic model		31
Time step [s]		0.0025

For each configuration five amplitudes and six dimensionless accelerations of the fairlead motion are combined to assess the line behaviour. The Table 4 shows the five amplitude ranges applied, equal for each mooring line shape. The amplitudes are defined from consistent ranges obtained from Suhara [26]experiments and DeepCwind tests [22]. Each amplitude is associated with the parameter Z_m, which is the maximum static vertical motion amplitude of the suspended segment of the line, shown in Table 4. The dimensionless acceleration (α) is defined in Eq. (5) from [26], and is set from 0.1 to 0.6 each 0.1. Then, the frequencies of the fairlead motion are obtained by Eq. (5). The range of the parameters used are common values in the reality. If we assume that the mooring analyzed is a 1:120 scaled line (about 180-200m sea depth), the amplitudes ranges are from 0.5 m to 4.3 m and the motion periods are from 3 to 30 seconds in a real scale.

$$\alpha = \frac{\omega^2 Z_m}{g} \tag{5}$$

Table 4: Fairlead amplitudes for each catenary configuration.

	Amplitude [m]	**S1 Zm [m]**	**S2 Zm [m]**	**S3 Zm [m]**
A1	0.0045	0.0280	0.0202	0.0140
A2	0.009	0.0560	0.0404	0.0280
A3	0.018	0.0840	0.0606	0.0420
A4	0.027	0.1399	0.1011	0.0700
A5	0.036	0.1959	0.1415	0.0980

4.2 Results and model comparison

Figure 6 shows the comparison of one cycle tension range for the six different shape-diameter configurations, for the given fairlead motion A4 amplitude and for the dimensionless accelerations 0.1, 0.2, 0.4 and 0.6. Also, the static tension is shown for the smallest acceleration case. The quasi-dynamic approach fits the dynamic model with a high degree of accuracy for the low acceleration ranges. Moreover, it also predicts the slack phenomenon as seen in C11 for α values of 0.4 and 0.6. For larger dimensionless accelerations the tension presents differences less than 32.5% on the peaks and the troughs, when the actual shape of the dynamics of the mooring lines differs to the static solution. Nevertheless, the overall shape and tension behavior is well fitted. Other differences that can be observed are the inner vibrations of the mooring line, which produce high frequency tension variations which are obviously not modelled in the quasi-dynamic approach.

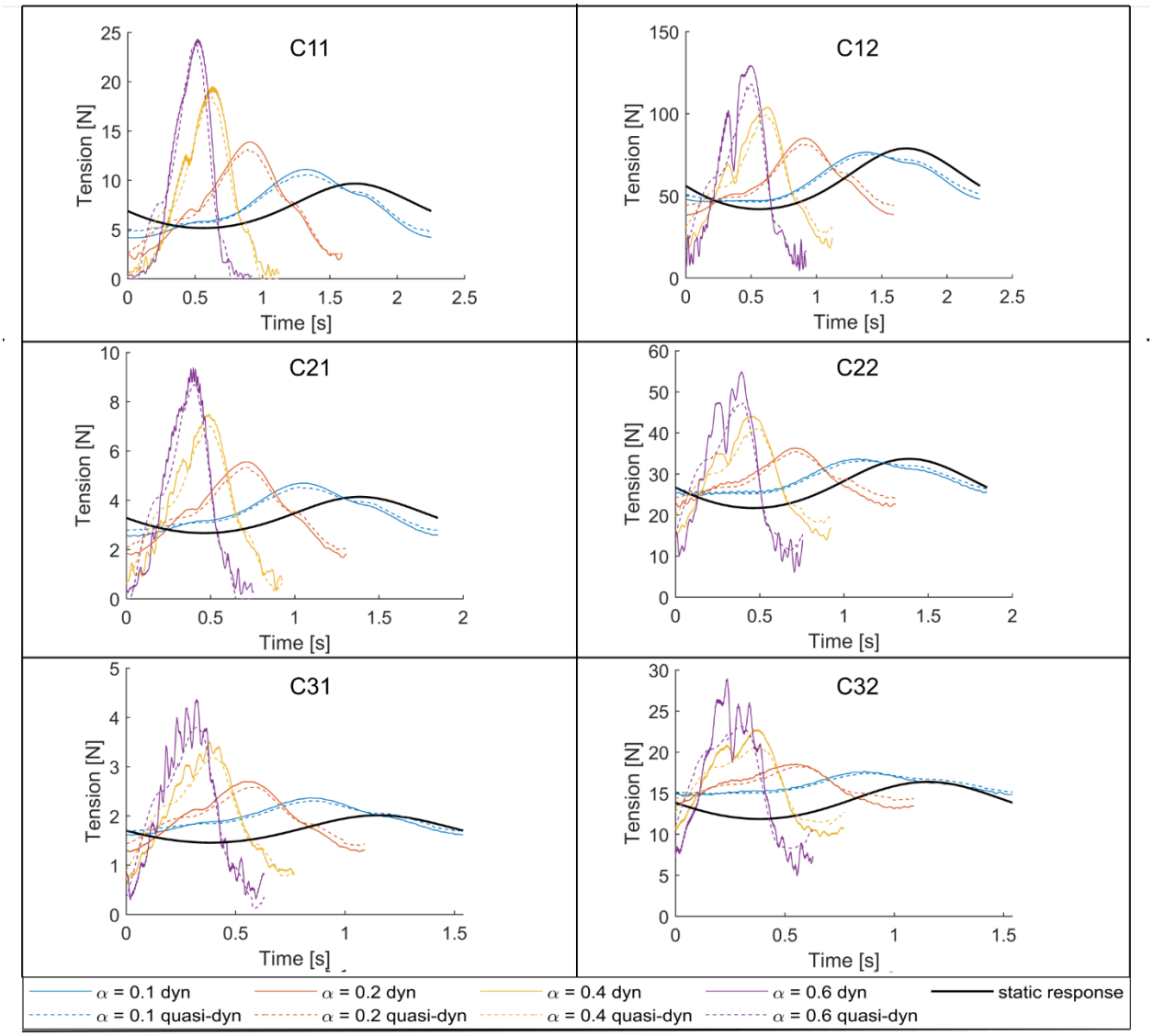

Figure 6: Tension comparison for amplitude 4 for the cases C11, C12, C21, C22, C31 and C32

An error analysis is performed in order to assess the differences between the dynamic model against the quasi-dynamic and the static models for all the simulations of verification. The error analysis consists in the assessment of the root-mean-square-error $(RMSE)$ of the fairlead tension for one cycle, and the assessment of the relative error (e) of the minimun and maximum peak tension at the fairlead.

The $RMSE$ is computed for the relative error of the quasi-dynamic and the static solutions, which are compared with the initial static force. The initial static tension $(T_{S,0})$ is used to avoid large relative errors for very low tension ranges. The $RMSE$ are presented in Eqs. (6) and (7) for the quasi dynamic and the for the static solutions respectively, where "i" is the assessed time step and "n" the total number of time steps assessed.

$$RMSE_{QD} = \sqrt{\frac{1}{n}\sum_{i=1}^{n}\left(\frac{T_{dyn,i} - T_{QD,i}}{T_{S,0}}\right)^2} \tag{6}$$

$$RMSE_{S} = \sqrt{\frac{1}{n}\sum_{i=1}^{n}\left(\frac{T_{dyn,i} - T_{S,i}}{T_{S,0}}\right)^2} \tag{7}$$

The results show the good accuracy of the quasi-dynamic model against the static solution in terms of both $RMSE$ (Figure 7) and the peak values (Figure 8). The $RMSE$ of the quasi-dynamic model is less than 10% for the 48% of all simulations, and less than 20 % for the 84% of all simulations. The error goes above 20% in the case of some slack events and the maximum error in terms of $RMSE$ is 37.6% (Figure 7-C11). The $RMSE$ of the static solution is less than 10% only for the 2 % of the simulations, and less than 20% for the 18% of the simulations.

The minum and maximum relative errors, Eqs. (8) and (9) respectively, are computed as the absolute value of the relative error of the local minimum and the local maximum, only for the quasi-dynamic model. The minimum relative error is assessed by comparing the error with the initial static tension $(T_{S,0})$ and the maximum relative error is assessed by comparing with the dynamic local maximum tension.

$$e_{Tmin} = \left|\frac{T_{min,dyn} - T_{QD,min}}{T_{S,0}}\right| \tag{8}$$

$$e_{Tmax} = \left|\frac{T_{max,dyn} - T_{QD,max}}{T_{max,dyn}}\right| \tag{9}$$

The maximum and minimum relative errors of the quasi-dynamic model have an error less of the 10% for the 67% of the simulations, and an error less than 20% for about the 90% of the simulations. Again, the error goes above 20% only in the case of large internal vibrations and the maximum error is 32.5% (Figure 8-C12).

If the errors are compared depending on the mooring line shape, the lower error are for the shape S3, then the S2 and finally the S1. As was expected, the increase of the suspened length also increases the motion of the line and the external forces. The errors also increase with the amplitude of the failread motion or the dimensionless acceleration. Again, as the energy of the excitation increase, the dynamic effects increase and the response of the mooring line clearly differs from the static line shape.

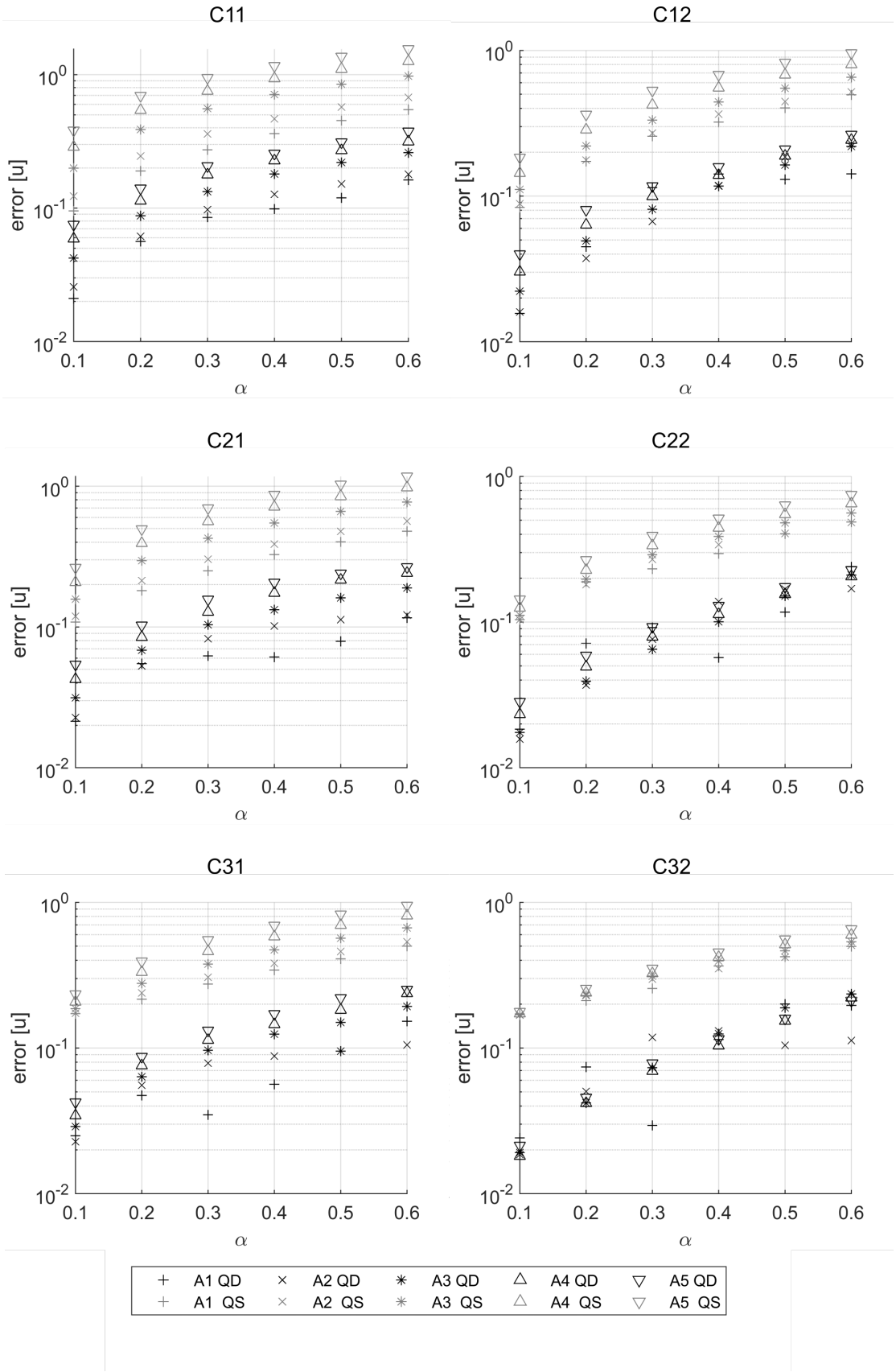

Figure 7: Root-mean-square-error

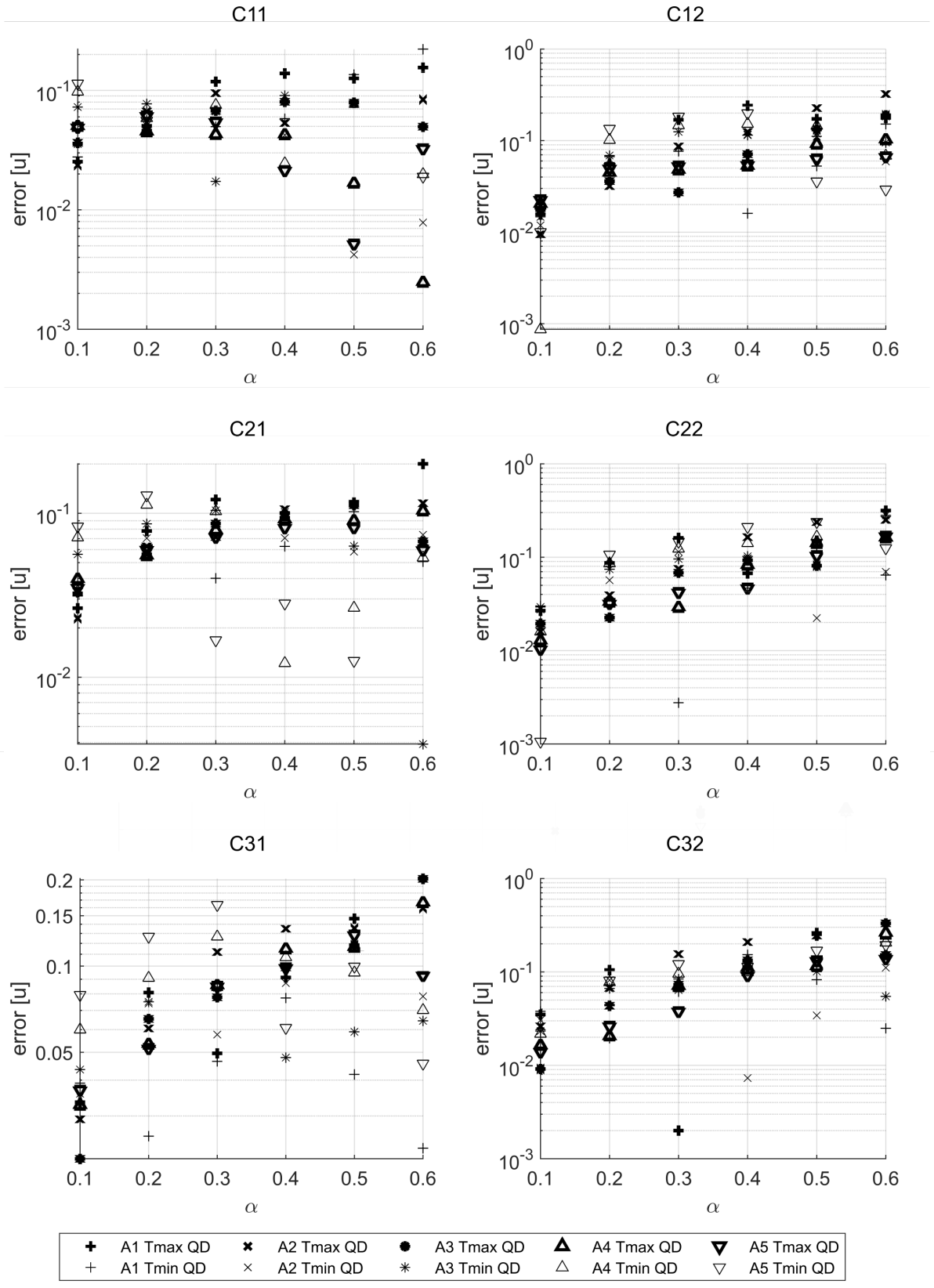

Figure 8: Minimum and maxim error comparison

5 MODEL VALIDATION

The main component for station keeping of the FOWTs is the mooring system. Although mooring systems are one of the most compliant components of a FOWT, the actual tension of the fairlead can change the motion of the platform, but normally is of little significance for the design loads of the platform. However, the actual tension of the mooring line is critical for the mooring design and can drive significant cost reductions if tension is reliably assessed.

The validation of the quasi-dynamic model is aimed to evidence the advantages, mostly improved accuracy and fast computation, of using of this approach in the coupled simulations for the mooring line design. The validation process is performed by comparing the experimental results of the DeepCwind platform with the numerical simulations using a mooring dynamic model, the quasi-dynamic proposed model and a quasi-static mooring model. Moreover, the Surge Free Decay is also used as a verification comparing the influence of the different mooring models in comparison with the experimental results. The floating platform is composed by 4 steel vertical pontoons connected by trusses, from where the central tower is connected (Figure 9 left). The $1/50^{th}$ scale model test of the concept was experimentally tested at the MARIN offshore basin [27,31] with a specifically built scaled wind turbine for the wave tank [32] (Figure 9 right). The experimental results were analyzed within the Phase II of the OC5 project [30].

The simulation performed corresponds to the load cases LC34 and LC43 of the OC5 Phase II project [22] with a depth of 200 m. In the load case 34 the platform is excited under the design wave state without wind, while in the load case 43, the platform is excited under an operational wave condition and a dynamic wind. The chosen simulations pretend to study the platform and the mooring system behavior under different load sources. In the wave only case, the LC34, the mean tension of the three lines will only differ due to the initial offset of the platform because no second order waves are applied and thus there is no drift force. Moreover, the platform will experience larger motions due to the larger waves and the lower stiffness performed by the mooring system in the surge direction. For the wind and wave case, LC43, the combination of the two main load sources of a FOWT are studied, which implies an increase of the low frequency loads due to the wind load in comparison with the LC34.

The simulations last 3h to ensure a full development of the irregular wave train, based on the Jonswap Spectrum, with a significant wave height (Hs) of 10.5 m and a peak period (Tp) of 14.3 s for the design wave state, and a significant wave height (Hs) of 7.1 m and a peak period (Tp) of 12.1 s for the operational wave. For the simulations, the second order wave forces are not considered. The dynamic wind has a mean wind speed of 13.05 m/s based on a NPD wind spectrum. The wind and wave are codirectional and aligned with the mooring line 2 and the X axis (Figure 9 bottom).

The FloaWDyn model is the aero-hydro-servo-elastic tool used for the simulations. The FloaWDyn model is based on a co-rotational Finite Element Model (FEM) developed at UPC Barcelona-Tech and is able to decouple the overall dynamics of the whole platform from its strains at each time step [17,33]. More details about the DeepCWind model in FloaWDyn can be found in [23].

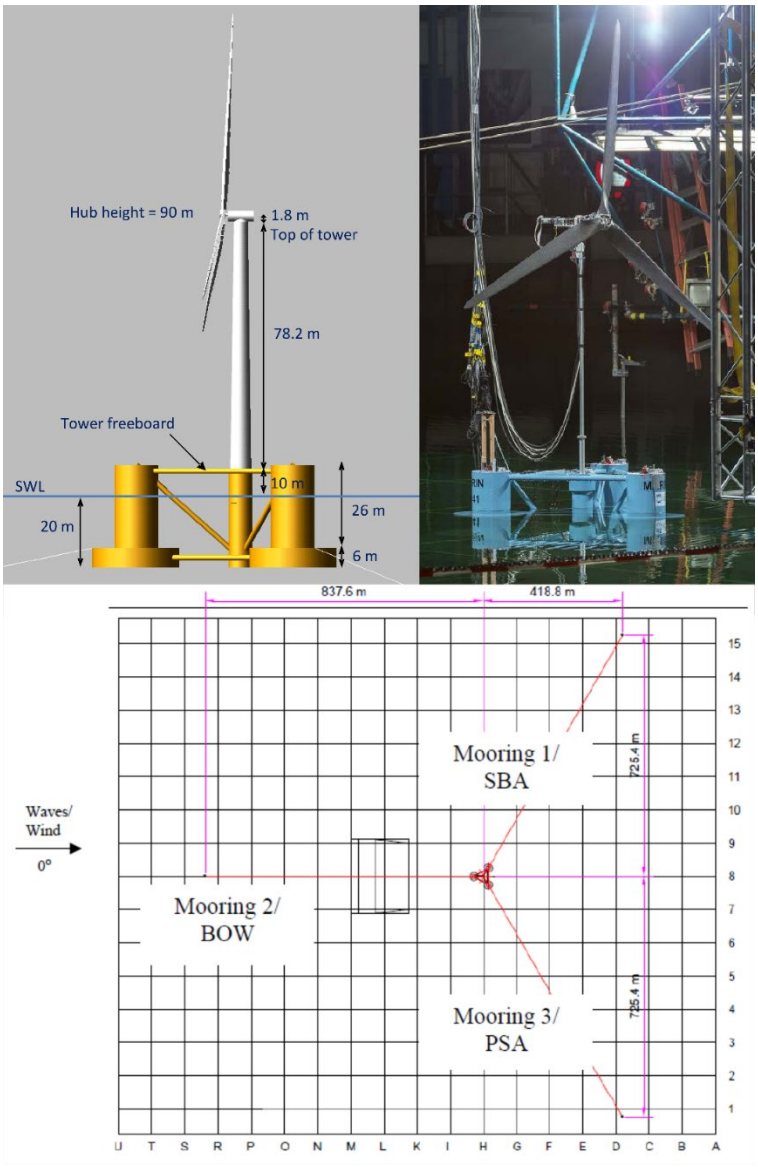

Figure 9:DeepCWind concept [34] *(left); OC5 task II Scale model* [27] *(right), Mooring line arrangement* [30] *(bottom).*

5.1 DeepCwind FloaWDyn Model

The DeepCwind model used for the simulations is the model set up at UPC for the OC5 Phase II project [33]. The platform plus the tower is modeled using 112 beam elements with 138 nodes. The mooring system is discretized in 60 elements, with 20 elements per line, and a total number of 63 nodes for the dynamic and the quasi-dynamic models.

Structural properties

The FEM beam model was adjusted, by adding the required ballast mass and adding lumped masses and inertias to specific nodes, to fit the main physical properties of the tested model, converted to full scale values (Table 5).

Table 5: DeepCwind test model prototype physical properties [23]

Mass [kg]	1.3958E+7
Draft [m]	20
Displacement [m^3]	1.3917E+4
CM below SWL [m]	8.07
Roll inertia about CM [$kg \cdot m^2$]	1.3947E+10
Pitch inertia about CM [$kg \cdot m^2$]	1.5552E+10
Yaw inertia about CM [$kg \cdot m^2$]	1.3692E+10

Hydrodynamic Properties

The hydrodynamic calibration of the model is set from the experimental free decay and regular wave tests. Since the hydrodynamics in the FloaWDyn code when using beam elements are based on the Morison's equation, the hydrodynamic coefficients to calibrate are the drag coefficients (C_d) and the inertia coefficients (C_m) for each structural member. Also, member added mass coefficients (C_a) are also adjusted to match with the total system added mass. The values used for the simulation are presented in Table 6.

The model takes also into account the diffraction of the waves by the MacCamy and Fuchs formulation [35,36].

Table 6: FloaWDyn DeepCwind Hydrodynamic coefficients [27]

	C_d		**C_a**		**C_m**	
	Trans	**Long.**	**Trans**	**Long.**	**Trans**	**Long.**
Upper Columns	0.600	--	0.52	--	1.5	--
Lower Columns	0.600	1.60	0.52	0.67	1.5	0.65
Tower Column	0.663	0.80	0.51	0.88	1.5	0.87
Cross-brace members	0.564	--	0.50	--	1.5	--
Mooring elements	1.880	0.86	0.50	--	1.5	--

Mooring properties

The characteristics of the mooring lines are described in Table 7. The three mooring lines are considered identical, instead of using different values for each line, by averaging the characteristics of the three lines. The hydrodynamic terms used are the tangential and normal drag coefficients (C_{dt}, C_{dn}) , the added mass term (C_a) and the inertia term $C_m = 1 + C_a$. The axial damping ratio (ξ_A) is set to 3%.

Table 7: Characteristics of DeepCwind mooring lines [23]

Number of mooring lines	3
Angle between adjacent lines	120º
Radius to anchors from centerline [m]	837.6
Radius to fairleads from centerline [m]	40.868
Unstretched mooring line length [m]	835.5
Nominal diameter [m]	0.0779
Volume-equivalent diameter [m]	0.1393
Mooring line mass density [kg/m]	125.6
Equiv. line extensional stiffness [N]	7.49E+8
Cdt	0.86
Cdn	1.875
Ca	0.5
ξ_A	3%
Number of nodes in the dynamic model	21
Integration points for the quasi-dynamic model	21

5.2 Results

5.2.1 Surge Free Decay

The Surge free decay test is performed by allowing the platform to move freely from an unbalanced surge position of 16.58m. The Figure 10 shows the comparison between the experimental data and the three mooring models. As expected, the quasi-static mooring model is the model that produces the lowest damping on the system due to the lack of mooring damping source. The dynamic and quasi-dynamic mooring models produces better results, with the dynamic one producing a little more damping than the quasi-dynamic one.

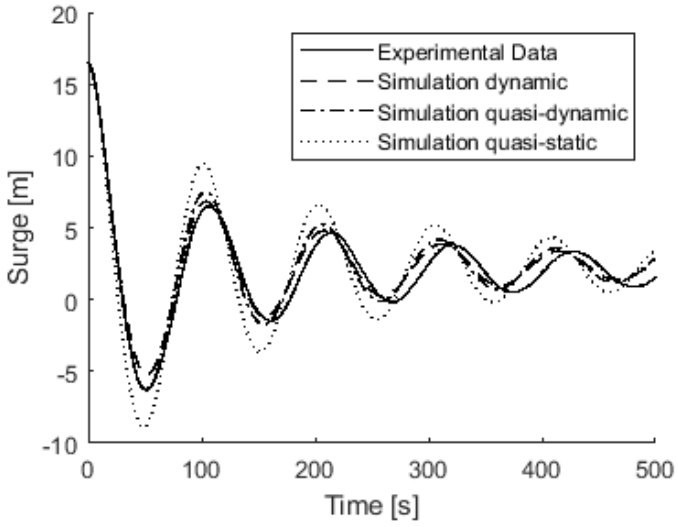

Figure 10: Surge Free-Decay comparison

5.2.2 Load Case 34: Waves only load case

- **Motion analysis comparison**

The surge, heave and pitch motions of the platform are compared by assessing the Power Spectral Density (PSD) (Figure 11). The results show a better accuracy for the quasi-static approach than the dynamic and quasi-dynamic models comparing with the experimental results, mainly for the low frequency range. This fact is a consequence of do not considering the low frequency wave loads in the simulations. Then, the dynamic and quasi-dynamic models damp the surge motion due to the lack of excitation in this range, whereas the quasi-static approach neglects the mooring line damping and fits better the experimental results.

The surge motion of the quasi-dynamic model produces values closer to the dynamic simulations than the quasi-static approach. However, the quasi-dynamic and dynamic approach produces a less accurate response to the experimental results for the low frequency range than the quasi-static approach. The heave motion of the quasi-dynamic and the dynamic models achieve a better response than the static one for the heave natural frequency at 0.057 Hz. The pitch response is quite similar for the three simulations but a close look reveals a more accurate results of the quasi-dynamic and dynamic simulations at the wave frequency range than the quasi-static response.

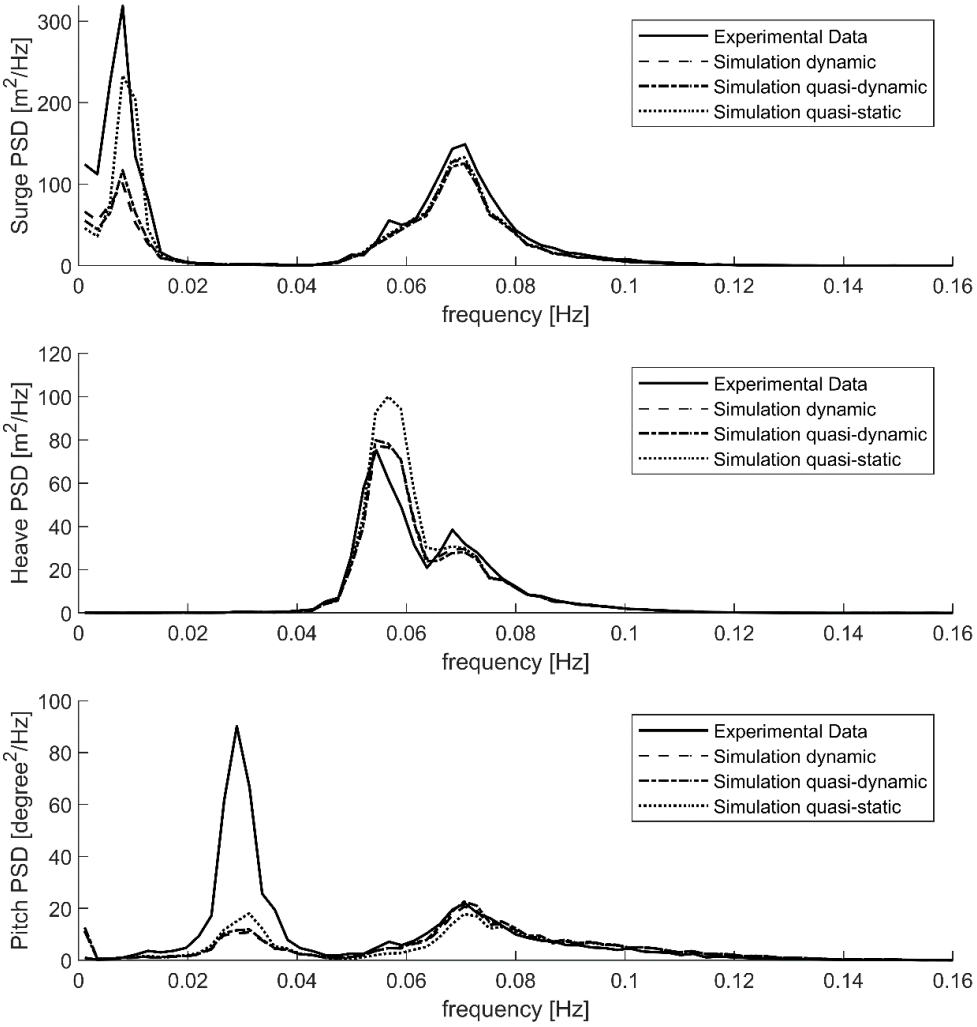

Figure 11: PSD the surge, heave and pitch motions of LC34

- **Tension analysis comparison**

Tension analysis is shown in the time domain (Figure 12), in the frequency domain (Figure 13) and a statistical comparison of mooring tension lines 1 and 2 is done (Table 8). Moreover, a study of the probability of exceedance of the minimum and maximum local tensions is performed and compared with the experimental data in Figure 14.

The statistical results of Table 8 show that the three models present good accuracy for the mean value of the tension, as only depends on the mean surge value of the platform which is low influenced by the dynamics of the mooring system. The standard deviation of the line tension (STD) is better fitted for the dynamic model for the two lines with an error of 13% for the line 2, and below 1% for the line 1. The STD error of the quasi-dynamic model is about 20% for both lines, and the quasi-static model presents the worst results with an error of 51% for the line 1, and an error of 73% for the line 2 respect to the experimental values. The difference of the STD error between the dynamic model and the quasi-dynamic model is lower for the line 2, which is 7%. The better performance of the quasi-dynamic model in the line 2 can be explained because the tension range is mostly due to the fairlead motion, whereas in line 1, the actual dynamics of the line, like the inner vibrations are proportionally larger, which are not captured by the quasi-dynamic model.

The peak tensions (maximum and minimum values) are well captured using the quasi-dynamic model, which produces results very close to the dynamic model and the experimental data.

Table 8: Statistical comparation of line tension of LC34

Line 1	**Mean Tension [kN]**	**STD [kN]**	**Min Tension [kN]**	**Max Tension [kN]**
Experiment	1.033e+03	7.658e+01	4.687e+02	1.342e+03
Dynamic model	1.030e+03	7.614e+01	4.722e+02	1.404e+03
Quasi-dynamic model	1.029e+03	6.129e+01	6.050e+02	1.372e+03
Quasi-static model	1.034e+03	3.772e+01	8.302e+02	1.189e+03
Line 2	**Mean Tension [kN]**	**STD [kN]**	**Min Tension [kN]**	**Max Tension [kN]**
Experiment	1.265e+03	4.481e+02	-3.171e+01	5.416e+03
Dynamic model	1.202e+03	3.920e+02	0.000e+00	4.625e+03
Quasi-dynamic model	1.199e+03	3.643e+02	0.000e+00	5.700e+03
Quasi-static model	1.193e+03	1.196e+02	9.096e+02	2.299e+03

The Figure 12 shows that the quasi-dynamic model fits very well with the dynamic model and the experimental data of tension in lines 1 and 2. For the lower excitation amplitudes. At the time range of 8380s-8420s three slack phenomena occur at Line 2. The quasi-dynamic model catches the three phenomena perfectly. However, the dynamic mooring approach better fits the experimental results, particularly after the post slack episode. Also, the peaks at the slack point are out of phase for the quasi-dynamic model. This phenomenon happens because there is no redistribution of the tension of the line that modifies the line shape from its static shape configuration, which slightly modify the peak time point. Nevertheless, if comparing with the quasi-static model, the results of the quasi-dynamic model are much better with a similar computational cost.

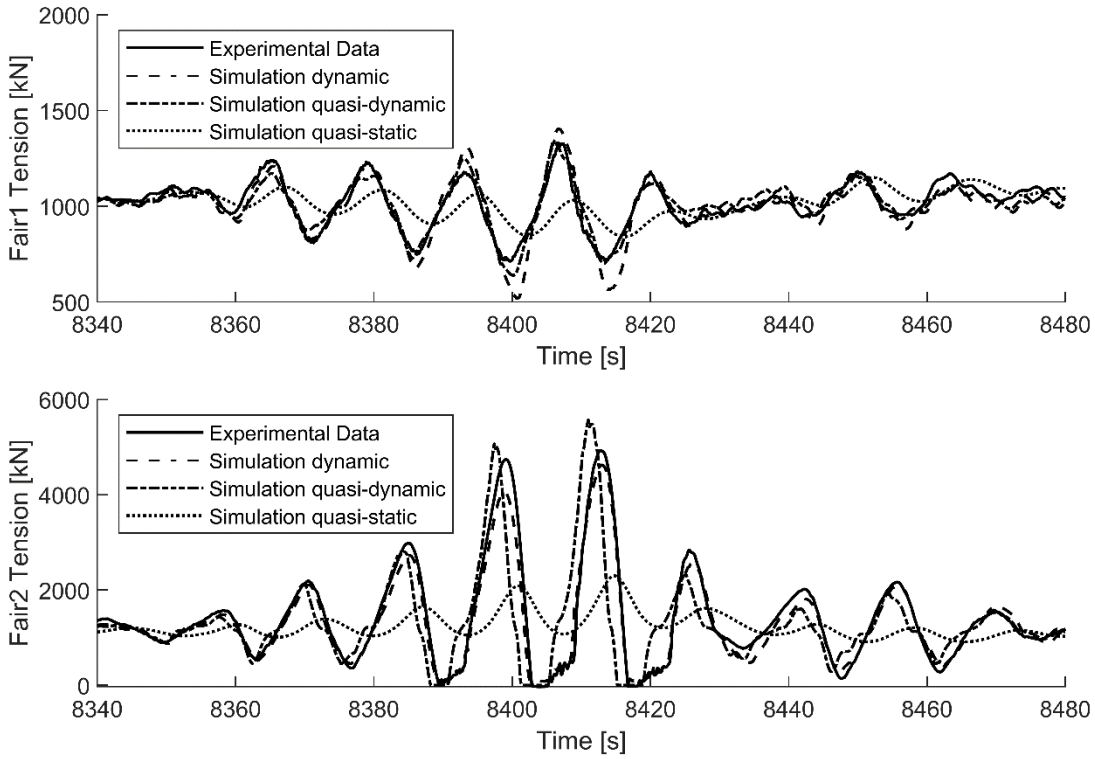

Figure 12: Tension time data comparison for LC34

The PSD of the tension at the fairlead of the mooring line 1 and 2 are presented in Figure 13. There is an evident improvement of the quasi-dynamic model compared with the quasi-static simulation in the wave frequency range. However, the energy of the PSD Tension in the wave frequency range of the quasi-dynamic model is smaller than the dynamic one. Moreover, the dynamic and the quasi-dynamic models underestimate the tension at the surge peak, within the low frequency range. The reason comes again from the low excitation of the surge frequency as the second order wave forces are not considered and the damping of the lines overdamps the motion compared with the quasi-static model, which has no damping source from the mooring lines.

The Figure 14 shows the probability of exceedance of the local minimum (left) and maximum (right) of the tension of the line 2. The probability of exceedance study shows clearly the underestimation of the tension computed by the quasi-static models. The quasi-dynamic model fits very well the minimum and maximum local values for the middle range values. However, the quasi-dynamic model overestimates the extreme tension values, both the minimums and maximums. This fact can be explained because these values occur at the slack phenomenon points when the mooring line reaches low tension values, and the quasi-dynamic model does not allow partial slackness of the mooring line. Moreover, after the slack events, the dynamics of the mooring line differs from the static shape, and the subsequent peaks are overestimated too.

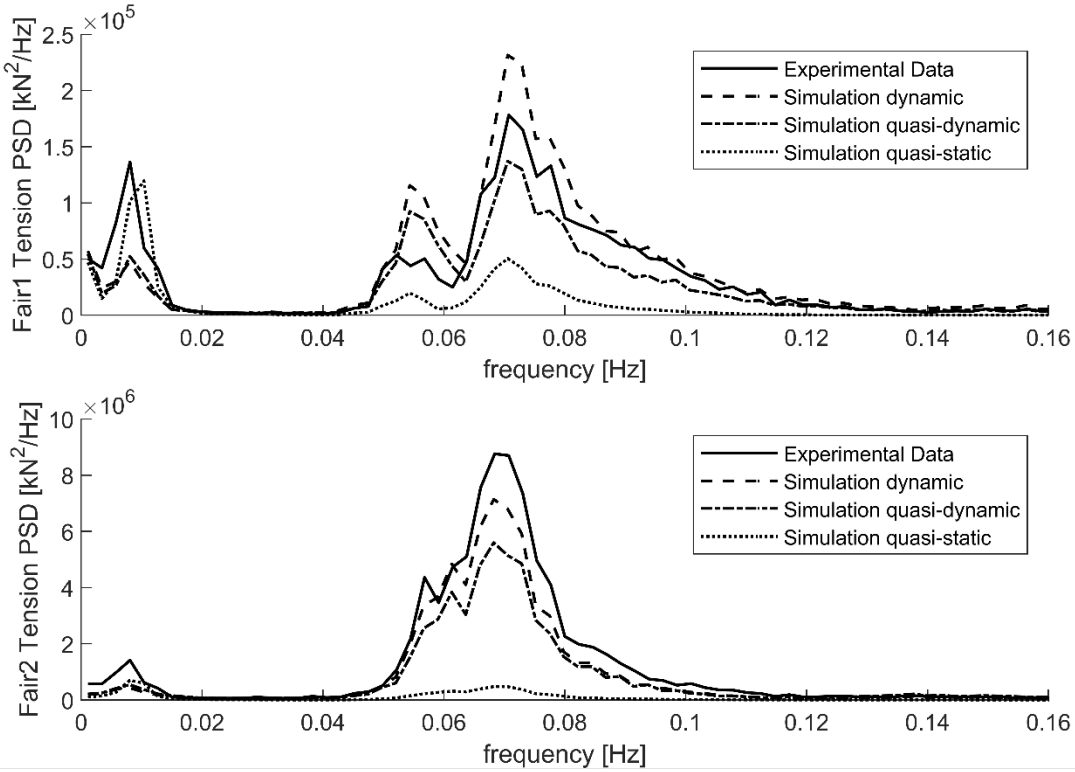

Figure 13:PSD of the Tension comparison of the LC34

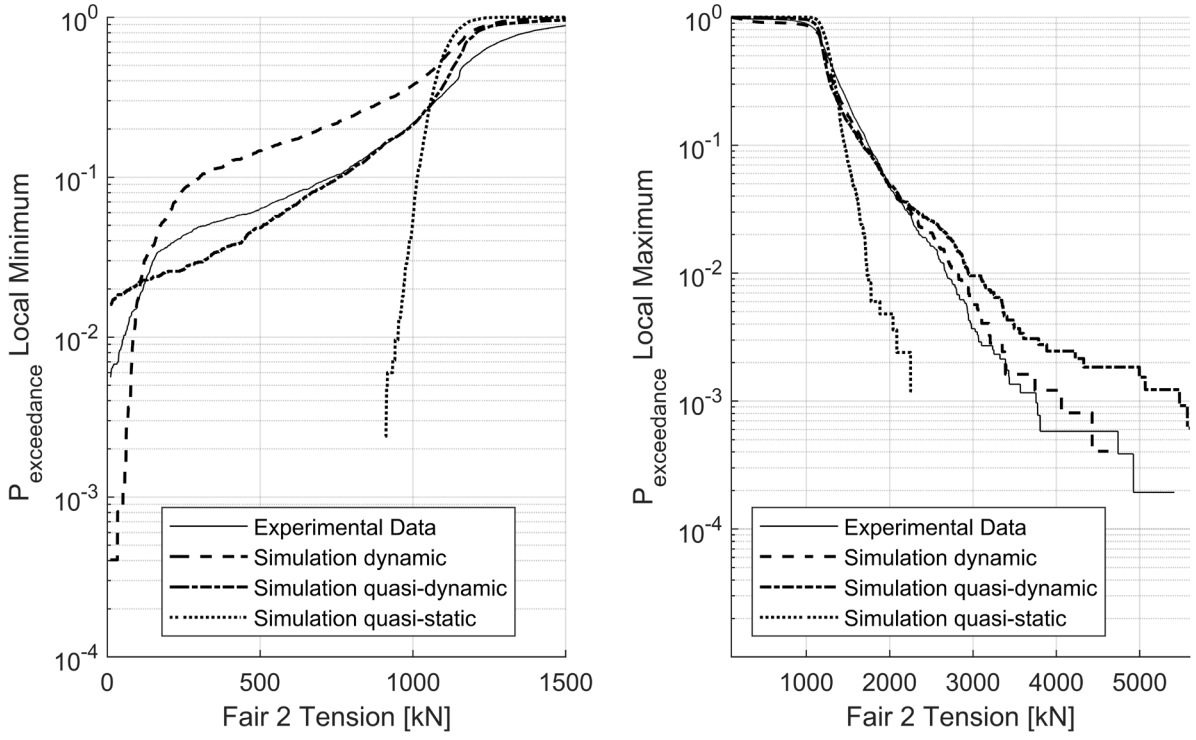

Figure 14: Probability of exceedance of mooring line 2 Tension for LC34

5.2.3 Load Case 43: Waves and wind load case

- **Motion analysis comparison**

The motions of the LC43 follow the same behavior of the LC34. The three models fit very well the experiment results for the wave frequency motion but differ for the low frequency range (Figure 15). As shown in Figure 11, the dynamic and quasi-dynamic mooring model present lower excitation in the surge low frequency range than the quasi-static model. Herein, also the lack of second-order wave forces induces and under-excitation of the surge motion. However, the difference between the experimental results is lower than in the LC34, because in this case, there is the wind low frequency excitation force which increase the loads in this range. On the other hand, the lack of mooring damping in the quasi-static model, which helps to fit the surge low frequency range, gives an over excitation in the heave frequency motion. Moreover, the differences in the damping of the surge and heave motion may be increased by the error on the mean position of the platform in the simulation compared with the experimental one, that lead to a shift on the mean tension values for the lines 1 and 2 as shown in Figure 16.

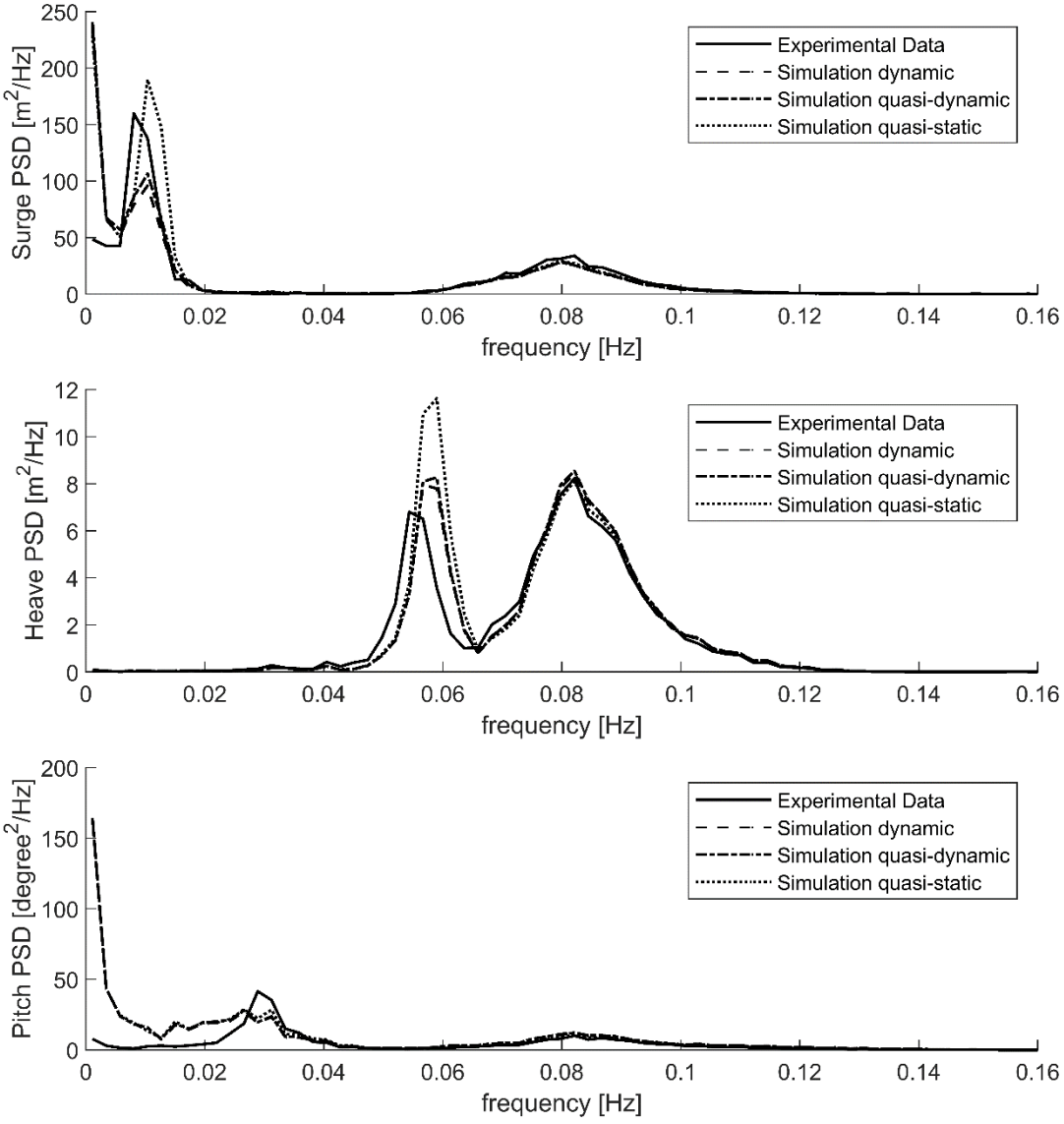

Figure 15: PSD the surge, heave and pitch motions of LC43

- **Tension analysis comparison**

The tension analysis comparison is performed again by a statistical analysis, by comparing the tension time data, by comparing the PSD response of the line tensions and by an analysis of the exceedance probability for the minimum and maximum peak values.

The statistical analysis is shown in Table 9. As stated previously, the mean values of the simulations differ slightly to the experimental results, because the mean position of the platform varied between tests [20] which is assumed to be due to an hysteresis phenomenon. The STD error of the Line 2 tension is of 0.2% for the dynamic model, 2% for the quasi-dynamic model and over 40% for the quasi-static model. For the Line 1 the STD error of the tension is of 15% for the dynamic model, 27% for the quasi-dynamic model and 42% for the quasi-static model. This analysis shows the good agreement of the quasi-dynamic model for the larger tensioned line. However, if the mean tension decreases, the error of the STD tension increases because the inner dynamic phenomena are not captured by the quasi-dynamic model and they are larger compared with the low external excitation tension of the line. The quasi-static model is the simulation with the poorest tension results compared with the experimental values.

Table 9:Statistical comparation of line tension of LC43

Line 1	**Mean Tension [kN]**	**STD [kN]**	**Min Tension [kN]**	**Max Tension [kN]**
Experiment	9.120e+02	4.418e+01	6.484e+02	1.119e+03
Dynamic model	8.510e+02	3.779e+01	6.428e+02	1.247e+03
Quasi-dynamic model	8.497e+02	3.230e+01	6.808e+02	1.092e+03
Quasi-static model	8.527e+02	2.545e+01	7.710e+02	1.056e+03
Line 2	**Mean Tension [kN]**	**STD [kN]**	**Min Tension [kN]**	**Max Tension [kN]**
Experiment	1.787e+03	3.125e+02	2.483e+02	4.254e+03
Dynamic model	1.987e+03	3.134e+02	5.193e+02	4.298e+03
Quasi-dynamic model	1.997e+03	3.065e+02	0.000e+00	5.246e+03
Quasi-static model	1.981e+03	1.775e+02	1.161e+03	3.064e+03

The Figure 16 shows the good agreement of the quasi-dynamic tension time data in comparison with the dynamic model results. On the other hand, the quasi-static model presents lower accuracy than the other models, with very low variation in the wave frequency range. The PSD comparison in Figure 17 certify the results found in the former analysis, where the quasi-dynamic model fits much better than the quasi-static approach, with larger accuracy for the larger tension line. At the low frequency range for the line 2, the dynamic and quasi-dynamic models fit better than the quasi-static approach. In this case, compared with the LC34, the second order wave forces are less important because there is the wind force acting on the low frequency range which reduces the error of the surge motion as seen in Figure 13.

On the other hand, the exceedance probability analysis shown in Figure 18 for the line 2 tension for LC43 has comparable results as the results of LC34. The quasi-dynamic model fits much better than the quasi-static approach, but presents larger exceedance probability for the smaller local minimums and larger local maximums. The differences between the experimental results and the dynamic approach can be explained by the lower accuracy of the model for the lager excitation mooring dynamic stages that produced the larger peaks and lower troughs.

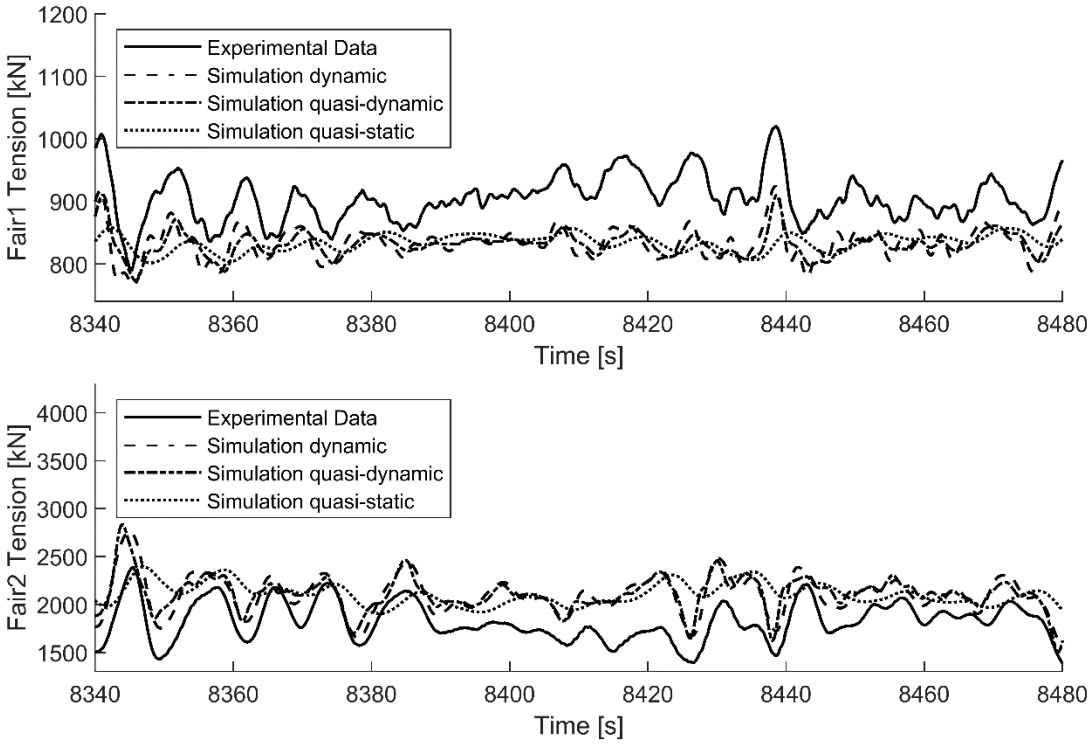

Figure 16: Tension time data comparison for LC43

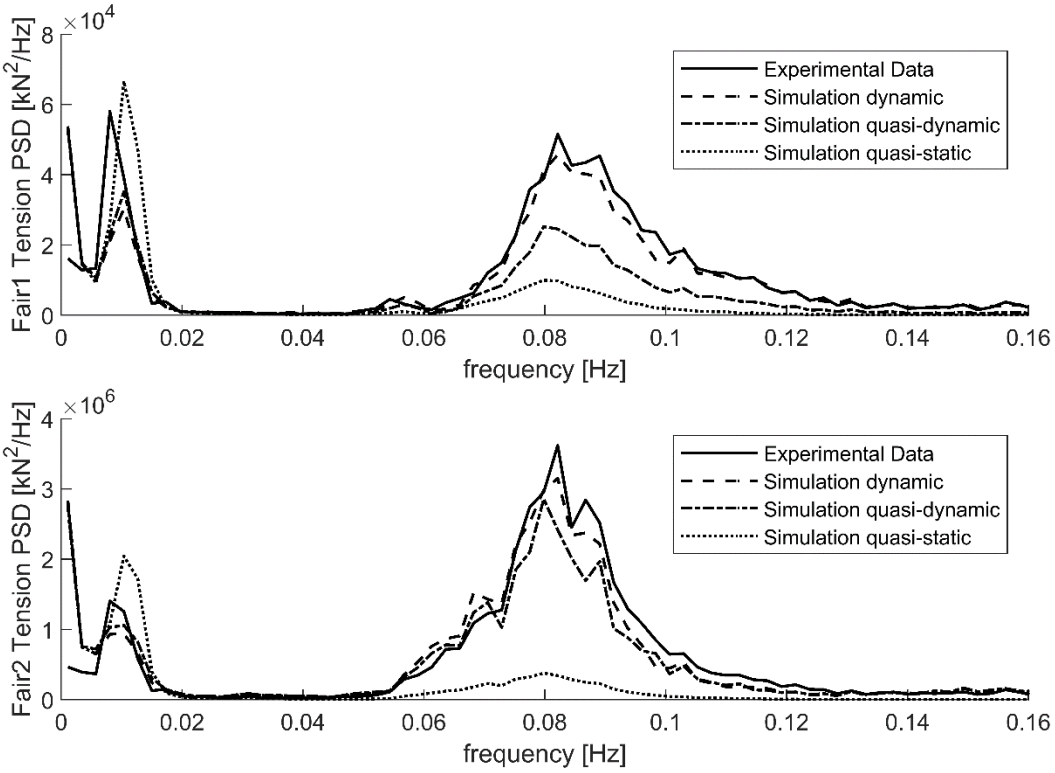

Figure 17: PSD of the Tension comparison of the LC43

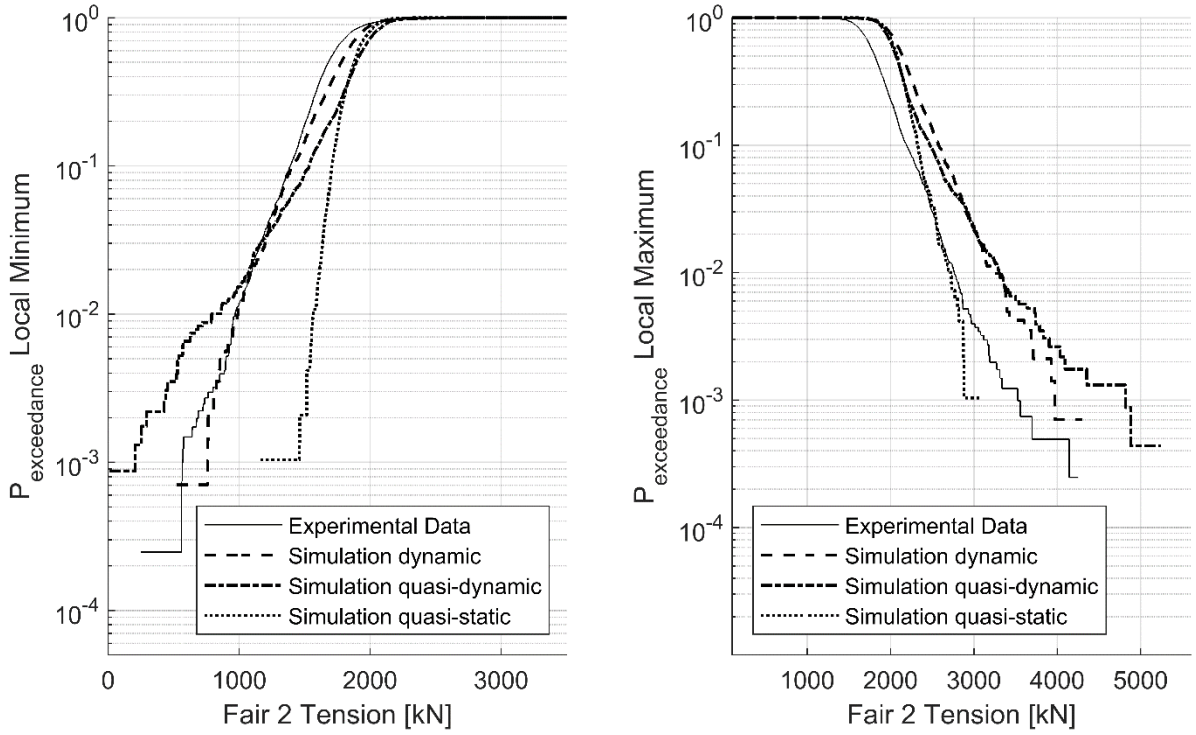

Figure 18: Probability of exceedance of mooring line 2 Tension for LC43

5.2.4 Fatigue analysis

This section aims to assess the fatigue damage produced in each line, for the studied load cases and for the different models as well as the experimental results.

The fatigue analysis is performed using DNV-GL mooring standard [24] and the rainflow counting ASTM methodology [37] to obtain the tension range. The rainflow method provides the number of cycles for the stress ranges for a time data stress history. The Figure 19 shows the histogram of the rainflow counting analysis, showing the cycle range, cycle average and the cycle counting.

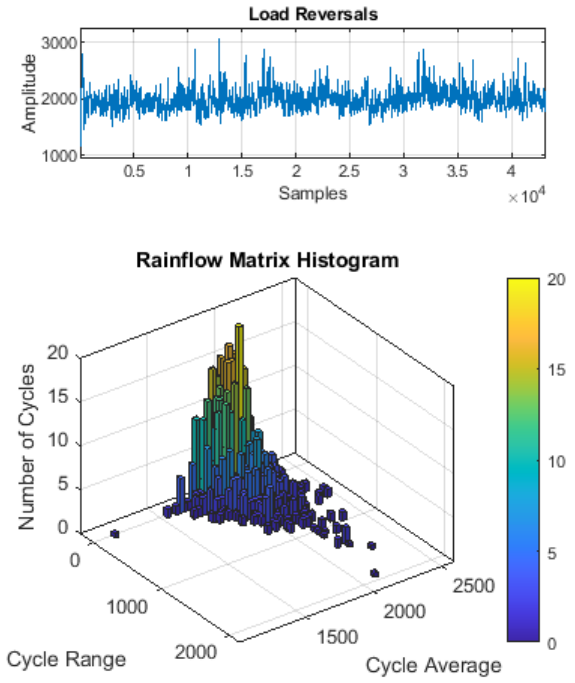

Figure 19: Rainflow histogram of mooring line 2 Tension of LC34

The damage of the mooring line in a state i (d_i) is assessed by Eq.(10).

$$d_i = \frac{n_i}{a_D} E[S_i^m \ ] \tag{10}$$

Where, n_i is the number of stress cycles, a_D is the intercept parameter of the S-N curve, m is the slope of the S-N curve, and $E[S_i^m]$ is the expected value of the nominal stres ranges raised to the power m in the state i.

Assuming that the mooring line is a studless chain, the a_D is set to 6.0E+10 and m is set to 3 [24].

The results of the damage assessed for each load case, for lines 2 and 3, for the experimental data, the dynamic, quasi-dynamic and quasi-static models are shown in Table 10. As expected, the quasi-static model gives the worst results of the three models compared with the experimental data underpredicting the damage produced at both lines for both load cases. For the most loaded line, line 2, the quasi-dynamic model fits better than the dynamic model comparing with the experimental results. This outcome, can be explained with the exceedance probability study. The quasi-dynamic model results overpredict the maximum tension in some peaks and the minimum tension in some troughs which lead to an increment of the tension range and an increase of the total damage of the line. This effect exceeds the total damage on the line for the quasi-dynamic model compared with the dynamic model. For the Line 1, the quasi-dynamic model underpredicts the total damage of the line, while the dynamic model fits better the damage assessed by the experimental data. Nevertheless, the damage produced at the line 1, which is the lowest loaded line, is about 100 times lower than the line 2 which is the most loaded one.

Table 10: Damage line comparison for LC34 and LC43

LC34	**Line 1**	**Line 2**
Experiment	1.764E-06	1.319E-04
Dynamic model	1.222E-06	2.202E-04
Quasi-dynamic model	4.264E-07	1.401E-04
Quasi-static model	8.488E-09	1.752E-07
LC43	**Line 1**	**Line 2**
Experiment	2.733E-07	6.527E-05
Dynamic model	1.685E-07	1.074E-05
Quasi-dynamic model	3.738E-08	7.266E-05
Quasi-static model	1.874E-09	1.596E-06

6 CONCLUSIONS

In this paper, the quasi-dynamic mooring model is presented, verified through a parametric study and validated by comparing it with experimental results.

The quasi-dynamic mooring model is based on the static catenary equation, where the solution is improved by applying a quasi-dynamic factor to the static tension. The quasi-dynamic factor accounts for the distributed weight, the inertial forces and the hydrodynamic forces over the suspended length of the line. The computation cost of the quasi-dynamic model is equivalent to the quasi-static ones, but is much less expensive than the dynamic mooring models.

The model fits very well the actual response of a mooring line for low and moderate fairlead excitation ranges with an error below the 10% compared with the dynamic solution. Moreover, the model is capable to predict the slack phenomenon. However, the actual behavior can be slightly different, for example the partial slack phenomenon of the line is not captured as well as its inner vibration.

The application of the proposed model is verified for a multiple motion ranges for six different mooring line configurations. The verification is performed by a parametric study varying the amplitude and the frequency of the motion. The results of the study show a clear improvement of the model against the static solution with an error below the 20% for the 85% of the simulations, whereas the quasi-static model presents an error below the 20% only for the 18% of the simulations.

The quasi-dynamic model is validated through the simulation of the DeepCWind semisubmersible and compared against the experimental data. The simulation results are also compared with the simulations of the platform with a dynamic mooring model and a quasi-static mooring model. Also, the influence of only wave load source or a combination of wind and waves are studied. The results show a very good improvement against the quasi-static approach, but, as could be expected, the proposed model is less accurate than the dynamic model. The model fits the mooring tension for low-middle motion ranges but overestimates the slack-snap phenomenon. The quasi-dynamic model works better for the larger tensioned and excited mooring line because the inner dynamics of the line are less important. Moreover, the study shows that the method becomes an efficient alternative to produce comprehensive fatigue assessments of the mooring lines because for the most loaded lines, the model achieves equivalent damage levels compared with the dynamic model.

REFERENCES

[1] Walton, T. S., and Polachek, H., 1959, *Calculation of Nonlinear Transient Motion of Cables*, Defense Documentation Center.

[2] Nakajima, T., Motora, S., and FujinoM., 1982, "On the Dynamic Analysis of Multicomponent Mooring Lines," OTC paper 4309.

[3] Ablow, C. M., and Schechter, S., 1983, "Numerical Simulation of Undersea Cable Dynamics," Ocean Engineering, **10**(6), pp. 443–457.

[4] Burgess, J. J., 1991, "Modeling of Undersea Cable Installation with a Finite Difference Method," *First International of Offshore and Polar Engng Conference*, pp. 2:222-227.

[5] Howell, C. T., 1992, "Investigation of the Dynamics of Low-Tension Cables," Massachsetts Institute of Technology.

[6] Gobat, J. I., and Grosenbaugh, M. a., 2001, "Application of the Generalized-α Method to the Time Integration of the Cable Dynamics Equations," Computer Methods in Applied Mechanics and Engineering, **190**(37–38), pp. 4817–4829.

[7] Garrett, D. L., 1982, "Dynamic Analysis of Slender Rods," Journal of Energy Resources Technology, **104**(4), pp. 302–306.

[8] Buckham, B. J., 2003, "Dynamics Modelling of Low-Tension Tethers for Submerged Remotely Operated Vehicles," University of Victoria.

[9] Palm, J., Eskilsson, C., and Bergdahl, L., 2017, "An Hp-Adaptive Discontinuous Galerkin Method for Modelling Snap Loads in Mooring Cables," Ocean Engineering, **144**(August), pp. 266–276.

[10] Petrone, C., Oliveto, N. D., and Sivaselvan, M. V., 2016, "Dynamic Analysis of Mooring Cables with Application to Floating Offshore Wind Turbines," Journal of Engineering Mechanics, **142**(3), p. 04015101.

[11] Azcona, J., 2016, "Computational and Experimental Modelling of Mooring Line Dynamics for Offshore Floating Wind Turbines," E.T.S.I. Navales (UPM).

[12] Trubat, P., and Molins, C., 2019, "Rheological Damping of Slender Rods," Marine Structures, **67**.

[13] Chakrabarti, S., 2005, *Handbook of Offshore Engineering*, Elsevier.

[14] Gobat, J. I., and Grosenbaugh, M. A., 2001, "A Simple Model for Heave-Induced Dynamic Tension in Catenary Moorings," Applied Ocean Research, **23**(3), pp. 159–174.

[15] Aranha, J. A. P., and Pinto, M. O., 2001, "Dynamic Tension in Risers and Mooring Lines: An Algebraic Approximation for Harmonic Excitation," Applied Ocean Research, **23**(2), pp. 63–81.

[16] Jonkman, B., and Jonkman, J., 2016, *FAST v8.16.00a-Bjj*, National Renewable Energy Laboratory.

[17] Campos, A., Molins, C., Trubat, P., and Alarcón, D., 2017, "A 3D FEM Model for Floating Wind Turbines Support Structures," *Energy Procedia*, Elsevier B.V., pp. 177–185.

[18] DNV GL, 2016, "DNVGL-ST-0437 Loads and Site Conditions for Wind Turbines," (November).

[19] Azcona, J., Palacio, D., Munduate, X., González, L., and Nygaard, T. A., 2017, "Impact of Mooring Lines Dynamics on the Fatigue and Ultimate Loads of Three Offshore Floating Wind Turbines Computed with IEC 61400-3 Guideline," Wind Energy, **20**(5), pp. 797–813.

[20] Robertson, A. N., Wendt, F., Jonkman, J., Popko, W., Gueydon, S., Qvist, J., Vittori, F., Uzunoglu, E., Yde, A., Galinos, C., Hermans, K., Bernardus, J., Vaal, D., Bozonnet, P., Bouy, L., Bayati, I., Bergua, R., Galvan, J., Mendikoa, I., Barrera, C., Shin, H., Molins, C., and Debruyne, Y., 2017, "ScienceDirect OC5 Project Phase II :

Validation of Global Loads of the DeepCwind Floating Semisubmersible Wind Turbine," Energy Procedia, **00**, pp. 1–19.

[21] Masciola, M., Robertson, A., Jonkman, J., Coulling, A., and Goupee, A., 2013, "Assessment of the Importance of Mooring Dynamics on the Global Response of the DeepCwind Floating Semisubmersible Offshore Wind Turbine," 23th International Offshore and Polar Engineering, **9**, pp. 359–368.

[22] Robertson, A. N., Wendt, F., Jonkman, J. M., Popko, W., Dagher, H., Gueydon, S., Qvist, J., Vittori, F., Azcona, J., Uzunoglu, E., Soares, C. G., Harries, R., Yde, A., Galinos, C., Hermans, K., de Vaal, J. B., Bozonnet, P., Bouy, L., Bayati, I., Bergua, R., Galvan, J., Mendikoa, I., Sanchez, C. B., Shin, H., Oh, S., Molins, C., and Debruyne, Y., 2017, "OC5 Project Phase II: Validation of Global Loads of the DeepCwind Floating Semisubmersible Wind Turbine," Energy Procedia, **137**, pp. 38–57.

[23] Trubat, P., Molins, C., and Gironella, X., 2019, "Wave Hydrodynamic Forces over Mooring Lines on Floating Offshore Wind Turbines," Ocean Engineering.

[24] DNV, 2010, "Offshore Standrad - Position Mooring," Det Norske Veritas, (DNV-OS-E301).

[25] Barrera, C., Battistella, T., Guanche, R., and Losada, I., 2020, "Mooring System Fatigue Analysis of a Floating Offshore Wind Turbine," Ocean Engineering journal, **195**.

[26] Suhara, T., Koterayama, W., Tasai, F., Hiyama, H., Sao, K., and Watanabe, K., 1981, "Dynamic Behavior and Tension of Oscillating Mooring Chain," Proceedings of the Annual Offshore Technology Conference, **1981**-**May**, pp. 415–418.

[27] Helder, J., and Pietersma, M., 2013, *DeepCwind/OC4 Semi Floating Wind Turbine Repeat Tests. MARIN Report No. 27005-1-OB*.

[28] DNV GL, 2018, "Offshore Standard - Position Mooring (DNVGL-OS-E301)," (July).

[29] Faltinsen, O. M., 1990, *Sea Loads on Ships and Offshore Structures*, Cambridge University Press.

[30] Robertson, A., Jonkman, J., Wendt, F., Goupee, A., and Dagher, H., 2016, *Definition of the OC5 DeepCwind Semisubmersible Floating System*, IEA.

[31] Goupee, A., Fowler, M., Kimball, R., Helder, J., and de Ridder, E., 2014, "Additional Wind/Wave Basin Testing of the DeepCwind Semi-Submersible With a Performance-Matched Wind Turbine," *Volume 9B: Ocean Renewable Energy*, p. V09BT09A026.

[32] de Ridder, E., Otto, W., Zondervan, G., Huijs, F., and Vaz, G., 2014, "Development of a Scaled-Down Floating Wind Turbine for Offshore Basin Testing," *Volume 9A: Ocean Renewable Energy*, ASME, p. V09AT09A027.

[33] Trubat, P., Campos, A., Molins, C., and Alarcón, D., 2017, "OC5 Task II Simulations with FloaWDyn Numerical Model," *Proceedings of the International Offshore and Polar Engineering Conference*, San Francisco.

[34] Robertson, A., Jonkman, J., Masciola, M., Song, H., Goupee, A., Coulling, A., and Luan, C., 2014, *Definition of the Semisubmersible Floating System for Phase II of OC4*, National Renewable Energy Laboratory.

[35] MacCamy, R. C., and Fuchs, R. A., 1954, "Wave Forces on Piles: A Diffraction Theory," U.S. Army coastal engineering Research Center (formerly Beach Erosion Board), Technical Memorandum No. 69.

[36] Trubat, P., Molins, C., Hufnagel, P., Alarcón, D., and Campos, A., 2018, "Application of Morison Equation in Irregular Wave Trains with High Frequency Waves," *Proceedings of the International Conference on Offshore Mechanics and Arctic Engineering - OMAE*, Madrid, pp. 1–10.

[37] ASTM E1049, 1985, "Standard Practices for Cycle Counting in Fatigue Analysis," ASTM Standards.